RSC Advances

PAPER

View Article Online
View Journal | View Issue

Cite this: *RSC Adv.*, 2021, **11**, 1086

Time-resolved detection of SDS-induced conformational changes in α-synuclein by a micro-stopped-flow system†

Shunki Takaramoto,[a] Yusuke Nakasone,[a] Kei Sadakane,[b] Shinsaku Maruta[b] and Masahide Terazima *[a]

An intrinsically disordered protein, α-synuclein (αSyn), binds to negatively charged phospholipid membranes and adopts an α-helical structure. This conformational change is also induced by interaction with sodium dodecyl sulfate (SDS), which is an anionic surfactant used in previous studies to mimic membrane binding. However, while the structure of the αSyn and SDS complex has been studied widely by various static measurements, the process of structural change from the denatured state to the folded state remains unclear. In this study, the interaction dynamics between αSyn and SDS micelles was investigated using time-resolved measurements with a micro-stopped-flow system, which has been recently developed. In particular, the time-resolved diffusion based on the transient grating technique in combination with a micro-stopped-flow system revealed the gradual change in diffusion triggered by the presence of SDS micelles. This change is induced not only by binding to SDS micelles, but also by an intramolecular conformational change. It was interesting to find that the diffusion coefficient decreased in an intermediate state and then increased to the final state in the binding reaction. We also carried out stopped-flow-kinetic measurements of circular dichroism and intramolecular fluorescence resonance energy transfer, and the *D* change was assigned to the formation of a compact structure derived from the helix bending on the micelle.

Received 12th November 2020
Accepted 18th December 2020

DOI: 10.1039/d0ra09614h

rsc.li/rsc-advances

Introduction

α-Synuclein (αSyn) is a protein of 140 residues localized at the presynaptic terminals of neurons.[1–3] The recombinant protein exists as a disordered monomer, and it is classified as an intrinsically disordered protein.[4] αSyn is a principal component of Lewy bodies, which are accumulated in the brains of patients with Parkinson's disease.[5,6] Recombinant human αSyn has been shown to form toxic oligomers and amyloid fibrils,[7,8] and binds to lipid bilayers or vesicles.[9,10] The conformation of αSyn depends on the environment; that is, it forms a random coil in aqueous solution, and mostly helical structures, particularly in the N-terminal region, upon association with negatively charged vesicles.[11–13] It has been reported that αSyn also interacts with micelles of anionic surfactants, such as sodium dodecyl sulfate (SDS), and forms an α-helical structure.[14] SDS has been widely used in biophysical studies to mimic the membrane interaction of αSyn.

Previous studies have shown that the natively unfolded structure of αSyn exhibits multistate folding from a random coil structure to an α-helical folded state with increasing concentration of SDS ([SDS]).[15,16] At a lower SDS/αSyn ratio, αSyn forms an incomplete helical form in the N-terminal region, and SDS molecules aggregate on αSyn. At this low concentration, αSyn tends to aggregate to ultimately form fibrils.[16–18] With increasing [SDS], αSyn forms an extended helix in the N-terminal region by forming a complex with SDS molecules.[19,20] At higher [SDS], αSyn interacts with micelles to form a bent (horseshoe) helix, which consists of two α-helices (Val^{3}–Val^{37}, Lys^{45}–Thr^{92}).[21] Moreover, not only the secondary structure, but also the overall structure of the protein–SDS complex, including the size and shape of the micelle around the protein, changes depending on [SDS].[16,18]

Although a number of previous studies elucidated the complex structure of αSyn and SDS, most of them have focused on the static structures under equilibrium conditions. The dynamics of the binding process from the monomeric disordered state to the micelle-bound state has not been elucidated. To understand the interaction between αSyn and anionic surfactants and associated conformational change at the molecular level, the dynamical behavior of the binding process

[a]*Department of Chemistry, Graduate School of Science, Kyoto University, Kyoto 606-8502, Japan. E-mail: mterazima@kuchem.kyoto-u.ac.jp*

[b]*Department of Bioinformatics, Graduate School of Engineering, Soka University, Hachioji, Tokyo 192-8577, Japan*

† Electronic supplementary information (ESI) available: Diffusion signal of NSP (Fig. SI-1), q^2 dependence of the TG signal of αSyn (Fig. SI-2), diffusion signals of bovine serum albumin labeled with NSP (Fig. SI-3). See DOI: 10.1039/d0ra09614h

needs to be clarified. In this study, the dynamics of the conformational change from the unstructured state of αSyn to the α-helix formation with the SDS micelle was studied using time-resolved measurements.

For the time-resolved detection of the reaction, a solution mixing method using a stopped-flow (SF) system combined with some spectroscopic techniques should be appropriate. To detect the association states and intermolecular interaction between αSyn and SDS, we probe the diffusion coefficient (D) in particular because this property is sensitive to these changes.[22,23] Therefore, the time-resolved diffusion (TRD) detection technique should be suitable for this work. However, with the traditional methods of D measurement, a longer time is required, and it has been impossible to trace the time course. The transient grating (TG) technique has changed the situation. Upon creating spatial modulations of concentrations of chemical species by pulsed light, D can be measured in a time-resolved manner. Utilizing high time resolution, this technique has been applied to studies on photochemical reaction mechanisms, including conformational changes during protein reactions.[24–27] Although this technique is powerful, the target reaction must be photo-initiated in principle. This restriction has limited the targets to photochemical reactions by the TG method. Here, we applied a recently developed technique, stopped-flow TG (SF-TG)[28] to detect the dynamics of αSyn-binding to the SDS micelle from the view point of diffusion. In the SF-TG technique, a reaction is triggered by mixing two solutions, and pulsed grating light is irradiated at various delay times to monitor D during reactions. There are two serious problems for applying this SF-TG to protein reactions by commercial SF systems; *i.e.*, sample volume and time resolution. Usually, it is difficult to prepare a large volume of protein samples, so that the solution volume for the SF system has to be very small. Furthermore, the time resolution of the TRD measurement is determined by a speed of the turbulent flow ending in the mixing chamber. To solve these difficulties, we have developed a micro-stopped-flow (μ-SF) system.[28] In this apparatus, the sample solution is introduced into the observation cell with high-pressure compressed air and mixed quickly in a micro-chamber. The total volume of the mixer and the observation window is about 3 μL, by which we can significantly reduce sample consumption. Furthermore, the small volume helps to stop the solution flow (turbulence) quickly.

Although we can start the reaction by solution mixing, photolabeling of the target protein is still necessary to detect diffusion of a protein by the TG method.[29] For this purpose, we labeled αSyn with a photoresponsive molecule. It is desirable to use a small molecule to avoid disturbing the target reaction and protein diffusion. Furthermore, the probe molecule should give rise to a strong TG signal. In our previous work, we have reported a candidate for such a purpose, that is, one of the spiropyran[30] derivatives, *N*-succinimidyl-3-[3,3-dimethyl-6′-nitrospiro[2′*H*-chromene-2,2'-(2,3,-dihydro-1*H*-indole)]-1 yl]-propionate (NSP) (Fig. SI-1A†).[31] In this work, for site-specific labeling of αSyn, another type of spiropyran derivative, 3-{3′,3′-dimethyl-6-nitrospiro[chromene-2,2′-indole]-1′-yl}-*N*-[2-(2,5-dioxopyrrol-1yl)ethyl]propanamide (DSP) was used. Upon photoexcitation of these dyes at 308 nm, the ring-closed spiropyran (SP) form is converted to the ring-opened merocyanine (MC) form, which gives rise to a strong TG signal. This DSP dye can label Cys residues. Since there is no Cys residue in αSyn, a Cys residue is added at the end of the C-terminal to label αSyn only at a specific point. Hereafter, we refer to this Cys-added αSyn as αSynC and that with DSP labeling as αSynCD.

In this study, the SF system was used not only for TRD detection, but also for stopped-flow kinetic measurement of circular dichroism (SF-CD) and Förster resonance energy transfer (SF-FRET). Combining these data, we elucidated the dynamical process of the αSyn binding reaction on the SDS micelle. This work clarified the micelle-binding dynamics involved in the secondary structure and intramolecular tertiary structure change of αSyn that occurs upon SDS binding.

Materials

Protein preparation

A Cys residue was added as a 141 residue at the end of the wild type human αSyn sequence for the TG measurement (αSynC), or a G7C/G84C double mutation was introduced for the FRET measurement. These mutants were generated by site-directed mutagenesis using the pET-28a plasmid. Recombinant αSynC and G7C/G84C mutants were expressed in *Escherichia coli* BL21 (DE3) strain transformed with the pET-28a vector. These proteins were produced by a purification protocol described previously[32] with some additional steps. Briefly, 1 L cultures (20 g tryptone, 10 g dried extract yeast, 5 g D-(+)-glucose, 5 g NaCl, 8.7 g K_2HPO_4, pH adjusted to 7.2) of *E. coli* were grown at 37 °C with shaking at 120 rpm and induced for expression of αSyn mutants when the OD_{600} reached 0.6–0.8 by 0.1 mM isopropyl-β-D-thiogalactopyranosid (IPTG). After 4–5 h of expression, the cells were pelleted by centrifugation. The mutants were released from the periplasm by the osmotic shock protocol. The supernatant was dialyzed overnight with 25 mM Tris–HCl, 5 mM dithiothreitol (DTT), pH 7.5, at 4 °C. The dialyzed solution was loaded on a Q-Sepharose column (Hitrap Q-HP, GE) equilibrated with 25 mM Tris, pH 7.5 running buffer, and eluted using a NaCl gradient. The purified fraction was boiled at 98 °C for 5 min. After the insoluble material was removed by centrifugation, the supernatant of αSynC was further purified by gel filtration with PBS buffer (pH 7.2). In the case of G7C/G84C, the supernatant was injected into a desalting column (Hitrap Desalting, GE) equilibrated with 25 mM Tris, pH 7.2. Before and after the ion exchange chromatography step, αSynC and G7C/G84C solutions were added to fresh DTT solution to prevent oxidization of the cysteine residues.

SDS was purchased from Nacalai Tesque, Japan.

Labeling by NSP and DSP

For diffusion measurements in SDS solution without the proteins, NSP was dissolved in *N*,*N*-dimethylformamide (DMF) at an initial concentration of 20 mM and it was mixed at 1 : 40 with 1 mM Tris in PBS buffer at pH 8.0. The mixed solution was incubated for 1 h, and the solution was filtered through

a Cosmospin Filter G (0.2 μm, Nacalai Tesque, Japan) to remove precipitates. For DSP labeling of αSyn, DSP was dissolved in DMF, and 200 μM αSynC solution was mixed with an equimolar ratio of DSP. The mixed solutions were incubated for 3 h at 23 °C. After purification by size exclusion chromatography, the protein concentration was determined by DcAssay (Bio-Rad). The fraction of the labeling was determined by absorption measurement using a U-1900 Spectrophotometer (Hitachi) (ε_{350} = 11 000 M^{-1} cm^{-1} for DSP and NSP[31]). The molar ratio of labeled DSP to αSyn was determined to be ~0.8. NSP was synthesized as reported previously.[31] DSP was synthesized by the coupling reaction of SP-COOH and *N*-(2-aminoethyl)maleimide with condensation reagent 1-ethyl-3-(3-dimethylaminopropyl)-carbodiimide (EDC). SP-COOH, 1-(β-carboxyethyl)-3,3-dimethyl-6-nitrospiro(indoline-2,2(2*H*-1)benzopyran) (57 μmol) was activated with EDC (68 μmol) in the presence of 3*H*-1,2,3-triazolo[4,5-*b*]pyridin-3-ol (68 μmol) in 0.8 mL DMF for 10 min at 25 °C. To this solution, *N*-(2-aminoethyl)maleimide (57 μmol) in 0.2 mL DMF was added and reacted for 10 min at 25 °C. The reactant was evaporated, and DSP was purified by flash column chromatography packed using a silica gel in a solvent of 20% methanol and 80% chloroform.

Labeling for FRET experiments

For FRET experiments, G7C/G84C mutant was labeled with Alexa Fluor 488 C5 maleimide (F488, donor) and Alexa Fluor 594 maleimide (F594, acceptor) dyes (Fluoroprobes, Scottsdale, USA). The G7C/G84C mutant at 200 μM was first mixed with a 1.5-fold excess of F594 in a solution of 4 M guanidine hydrochloride, 500 μM tris(2-carboxyethyl)phosphine, and 25 mM Tris at pH 7.2, and the mixture was incubated at 4 °C overnight in the dark. The product was purified using a desalting column (HiTrap Desalting). The molar ratio of F594 to the protein was estimated to be approximately 1.4, based on the absorption (ε_{590} = 92 000 M^{-1} cm^{-1}). This ratio indicated that there were unlabeled sites in the protein. Then, this protein solution was mixed with a 5-fold excess concentration of F488 to produce a double-labeled protein. After unlabeled dye molecules were removed by desalting column chromatography (HiTrap Desalting), further purification was conducted using size exclusion chromatography (ENrich SEC 650 10 × 300 Column). The labeled protein concentration was determined by DcAssay. The molar ratio of labeled F594 to F488 was determined to be 1.5–2 using ε_{494} = 73 000 M^{-1} cm^{-1} of F488. The sample should be a mixture of 7C-F488/84C-F594, 7C-F594/84C-F488, and 7C-F594/84C-F594 proteins. A double-F488-labeled protein may also exist in the sample. However, its fraction was expected to be smaller than those of others, because most of the protein was labeled by F594 in the first labeling step.

Measurements

In all the spectroscopic measurements, PBS buffer (10 mM Na_2HPO_4, 1.8 mM KH_2PO_4, 137 mM NaCl, and 2.7 mM KCl, pH 7.5) at 295 K was used. The concentration of αSynC, αSynCD, or G7C/G8 labeled with the fluorescent dyes was determined by DC assay.

TG measurement. The experimental setup for the TG measurement was similar to that reported previously.[33] Briefly, an excimer laser (Lamda Physik Compex 102) at 308 nm was used for excitation. The excitation beam was split into two by a beam splitter and crossed inside a sample cell (an optical path length of 2 mm) for static measurements or inside the mixing chamber for kinetic measurements. In all the experiments, a continuous-wave laser of a He-Ne laser (1144P, JDS Uniphase) was used for the probe beam. The TG signal was detected by a photomultiplier tube (H7422-20, Hamamatsu Co.) and recorded using a digital oscilloscope (DSO9054H, Agilent Technology). In the static measurement, the repetition rate of photoexcitation was 0.05 Hz. After every excitation and measurement, the sample solution was exposed to a diode laser light at 449 nm (L4 445-38 TE, Micro Laser Systems, Inc.) or LED (480 nm) (B3VP-8, NISSIN ELECTRONICS) for 20 s to recover the SP form. The sample solutions were filtered using a 0.2 μm syringe or spin filter before the measurements. A protein concentration of 20 μM was used for static measurement in a quartz cell. For SF-TG measurement, an equal amount of the two solutions of 40 μM αSynCD and 6 mM SDS were mixed to achieve 20 μM αSynCD and 3 mM SDS solution.

CD measurement. The CD spectrum was measured by a CD spectrometer (J-720WI, JASCO) in a quartz cell with an optical path length of 0.2 mm. The accumulation of SP or MC state of labeled protein were achieved by irradiation of the LEDs (480 nm or 365 nm) for 1 minute. The protein concentration of 20 μM was used for a static measurement in a quartz cell. For SF-CD measurement, an equal amount of the two solutions of 40 μM αSynC and 6 mM SDS were mixed to achieve 20 μM αSynC and 3 mM SDS solution.

FRET measurement. The fluorescence spectrum was measured using a fluorescence spectrometer (FP-777, JASCO) at an excitation wavelength of 449 nm (bandwidth, 5 nm), and with a 470 nm long-pass filter in front of the detector. Previous studies have shown that physical properties depend on the relative concentration of αSyn against [SDS].[16,19,21] Hence, a protein concentration of 20 μM, which was used for the TG and CD measurements, was also used in the FRET experiment. However, since it was difficult to prepare such amount of the F488–F594 double-labeled protein, the labeled protein of 0.5 μM was mixed with 20 μM αSynC for the FRET experiment following the previous FRET experimental protocol.[19] This dilution of the labeled protein may also help to avoid possible intermolecular energy transfer.

Stopped-flow measurements. In the SF-TG and SF-FRET measurements, protein solution at 40 μM and SDS solution were mixed using the μ-SF system (optical path length, 0.8 mm). The mixing procedure was almost the same as that reported before.[28] Briefly, two sample solutions were mixed in the observation cell using high-pressure air (4 bar) with a compressor (DP0105-Y1-0001, Nitto Kohki) and a plunger pump (LPVA1700330H, Lee Co.). The start and stop times of the flow were regulated by four two-way valves (MTV-2SL-N32UF, Takasago Electronics). The diameter of the mixing part was

0.26 mm. An observation cell was a rectangular hole with dimensions of 0.8 × 0.8 × 3.0 mm (Japan Cell). The mixing ratio of the two solutions was 1 : 1.

In the SF-TG experiment, the signals were measured 20 times at each delay time, and the signals were averaged later.

In the SF-FRET experiment, laser light at 449 nm was focused on the mixing chamber of the μ-SF system. The fluorescence of F594 was detected by a photomultiplier tube with a 600 nm long-pass filter. The time-dependent fluorescence intensity after mixing solutions was detected 40 times for each [SDS], and the signals were averaged later. Background scattering light was detected for the PBS buffer without the labeled protein, and the signal was subtracted from the data. The dead time for the fluorescence measurement was ~400 μs.[28]

Kinetic far-UV CD measurements (SF-CD) were carried out using an RX-2000 stopped-flow apparatus (Applied Photophysics, optical path length, 2 mm) and a CD spectrometer. In the SF-CD measurement, the reaction was initiated by mixing 40 μM protein solution and 6 mM SDS solution with a mixing ratio of 1 : 1. In the SF-CD measurement, the CD intensity at 222 nm (bandwidth, 5 nm) was monitored with a response time of 32 ms. The protein concentration was 20 μM. For each [SDS], the SF-CD signal was recorded 10 times, and the signals were averaged later.

Principle of TG method

The principle of the TG method has been reported before.[34] Briefly, upon photoexcitation of the solution by the grating light, the sinusoidal modulations of the concentrations of the reactant and the product are created to lead the sinusoidal modulation in the refractive index (δn). Under the present experimental conditions, the signal solely consists of the thermal grating ($\delta n_{th}(t)$) and created (or depleted) chemical species by the photoreaction (species grating). The species grating signal intensity is given by the difference of the refractive index changes from the reactant ($\delta n_R > 0$) and the product ($\delta n_P > 0$). If the photoreaction is fast enough and D is time-independent in the observation time window, the TG signal ($I_{TG}(t)$) is expressed as

$$I_{TG} = \alpha\{\delta n_{th} \exp(-D_{th}q^2t) + \delta n_P \exp(-D_Pq^2t) - \delta n_R \exp(-D_Rq^2t)\}^2 \quad (1)$$

where α is a constant, D_{th} is the thermal diffusivity of the solution, D_P and D_R are the diffusion coefficient of the photoproduct and reactant, and q is the grating wavenumber. If D of the product is the same as that of the reactant, the observed profile derived from the species grating is given by a single exponential function.

Micelle formation in SDS solution

The critical micelle concentration (cmc) of SDS under the present experimental conditions was measured using the diffusion detection of NSP. Since NSP is a hydrophobic probe, it partly exists in the SDS micelle. D was measured using the TG method. A typical TG signal of NSP at 20 μM in the PBS buffer upon photoexcitation of the SP form probed at 633 nm and $q^2 = 3.6 \times 10^{12}$ m^{-2} is depicted in Fig. SI-1A.† The signal rose with a response time of our system, decayed to the baseline in the microsecond time region, and showed a slower decay profile. The faster decay component is the thermal grating signal, which decays with the rate constant of $D_{th}q^2$. The slower one corresponds to the NSP diffusion signal, and it was well reproduced by a single exponential function, indicating $D_P = D_R$ in eqn (1). From the decay rate constant, D of NSP (D_{nsp}) was determined to be $(3.8 \pm 0.1) \times 10^{-10}$ m^2 s^{-1}.

When SDS was added to the NSP solution, the decay rate of the diffusion signal did not change much until 1.0 mM SDS. With increasing [SDS] more than 1.3 mM, the decay became slower (Fig. SI-1B and C†). This slower decay indicates that the diffusion of NSP becomes slower due to micelle formation. The TG signals at higher [SDS] were fitted by eqn (2),

$$I_{TG} = \alpha\{\delta n_{nsp} \exp(-D_{nsp}q^2t) + \delta n_{mic} \exp(-D_{mic}q^2t)\}^2 \quad (2)$$

where D_{nsp} and D_{mic} are D of NSP in the buffer solution (free NSP) and that in the micelle, respectively. Furthermore, δn_i (i = nsp, and mic) is the refractive index change of these states. For the fitting of the signals, D_{nsp} is fixed to 3.8×10^{-10} m^2 s^{-1}, which is determined above. By using global fitting, the signals in an SDS concentration range of 2–50 mM can be reproduced well with a constant D_{mic} of $(1.2 \pm 0.1) \times 10^{-10}$ m^2 s^{-1}. The determined D_{mic} agrees well with previously reported values in the presence of NaCl (1.2 to 1.3×10^{-10} m^2 s^{-1}).[35] On the basis of these observations, the cmc of SDS was estimated to be ~1.3 mM, which agrees well with values in the literature (0.75 mM, 1.73 mM).[16,36]

Result

SDS-induced helix formation of αSyn

First, the influence of the labeling on the secondary structure of αSyn was examined by the CD spectra under static conditions. In the absence and presence of SDS, the CD spectra of αSynC and αSynCD at 20 μM are shown in Fig. 1A. Both spectra are almost identical and very similar to those reported previously for αSyn,[15] indicating that Cys addition and DSP-labeling do not introduce perturbations in structural properties of the protein. This observation is reasonable, because αSyn binds to SDS in the N-terminal region.

With the addition of SDS, the signal intensity of CD increases, indicating an increase in the α-helix content (Fig. 1A and B). This increase is independent of the state of DSP (MC or SP) (Fig. 1B), indicating that labeling by DSP and the photoconversion (SP to MC state) of DSP do not prevent αSyn adopting N-terminal helical conformation. Fig. 1C shows the [SDS] dependence of the CD intensity at 222 nm. The CD intensity is strong at 1–2 mM SDS, slightly decreases at 3 mM, and remains almost constant in the higher concentration region (Fig. 1C). This behavior agrees well with previous reports.[15,16] The increase in the CD intensity at 1 mM can be explained by α-helix formation in the N-terminal region of αSyn. The subsequent decrease from 2 to 3 mM is assigned to the

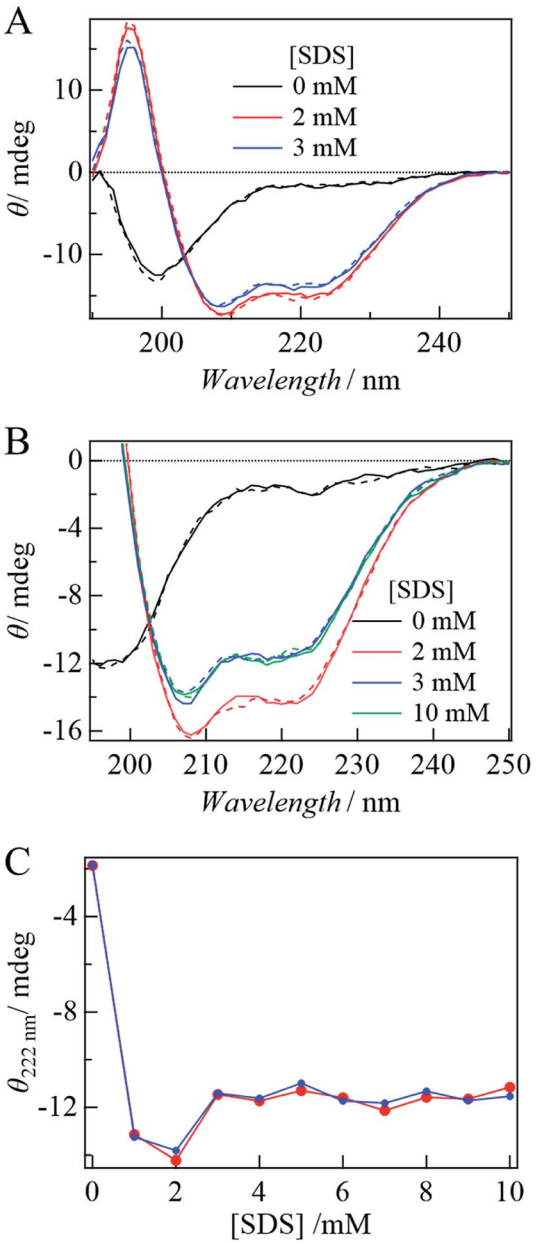

Fig. 1 (A) CD spectra of αSynC (broken lines) and αSynCD (solid lines). (B) [SDS] dependence of CD spectra of αSynCD in the SP form (solid lines) and the MC form (broken lines). (C) Plot of ellipticities of αSynCD at 222 nm against [SDS] in the SP (blue) and MC forms (red).

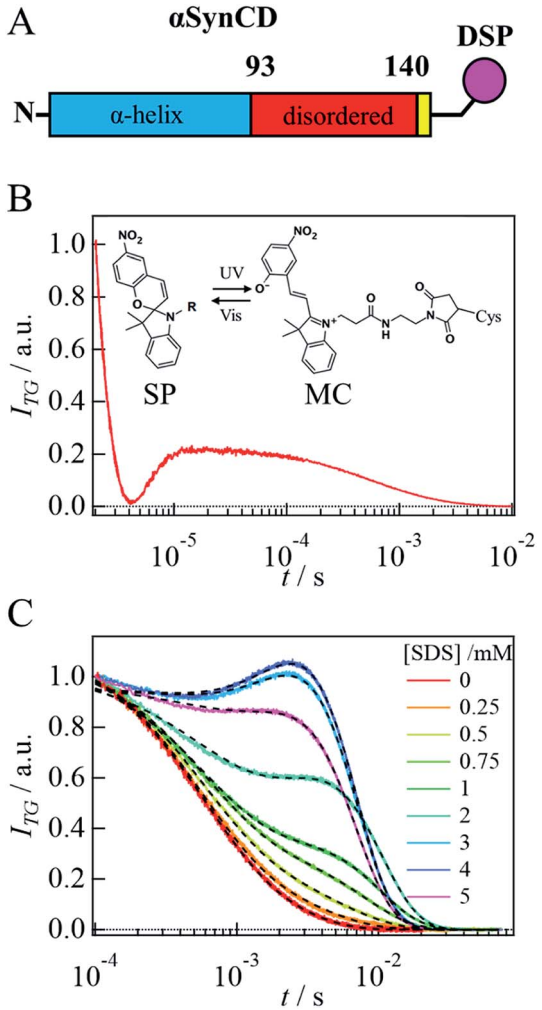

Fig. 2 (A) The domain structure of αSynCD. Added cysteine residue (141C) is shown by the yellow part. (B) A typical TG signals of αSynCD without SDS at $q^2 = 3.5 \times 10^{12}$ m^{-2}. An illustration of the photo-conversion of the labeled DSP is inserted. (C) SDS dependence of the diffusion signals of αSynCD at $q^2 = 3.5 \times 10^{12}$ m^{-2}. The fitted curves by eqn (3) for [SDS] = 0 mM and eqn (4) for the others are shown by the broken lines.

change of the α-helix from an elongated state to a bent horse-shoe helix form.

Complex formation of αSyn with SDS by static diffusion measurement

We probed the effect of SDS on D of αSynCD (Fig. 2A) using the static TG technique. In the absence of SDS, the signal showed two decay components consisting of the thermal and species gratings (Fig. 2B). The species grating signal is fitted by a sum of two exponential functions;

$$I_{\mathrm{TG}} = \alpha\{\delta n_{\mathrm{s}} \exp(-D_{\mathrm{s}} q^2 t) + \delta n_{\mathrm{f}} \exp(-D_{\mathrm{f}} q^2 t)\}^2 \quad (3)$$

where δn_{i} and D_{i} (i = s and f) are the refractive index change and D of the i-species, respectively, and the subscripts s and f denote the slower and faster decay components, respectively. Since D_{f} is found to be close to D_{nsp} (3.8×10^{-11} m^2 s^{-1}) by a preliminary fitting, the faster component is attributed to the diffusion of residual free DSP in the solution. Hence, we fixed $D_{\mathrm{f}} = 3.8 \times 10^{-10}$ m^2 s^{-1} during the fitting process to reduce the ambiguity of the fitting parameters. By this method, $\delta n_{\mathrm{s}}/\delta n_{\mathrm{f}}$ and D_{s} are determined to be 3.0 and 7.0×10^{-11} m^2 s^{-1}, respectively. The determined D_{s} is close to that of αSyn reported previously (6 to 7 $\times 10^{-11}$ m^2 s^{-1}).[18,37,38]

Addition of SDS to the solution changes the diffusion signal. A characteristic rise-decay profile appears and gradually increases with increasing [SDS] (Fig. 2C). The rise-decay curve

implies that the D_P and D_R of αSyn in eqn (1) are different. Based on the fact that δn_{th} is negative, we determine the signs of the decay and rise components to be positive and negative, respectively. Hence, the decay rate represents $D_P q^2$ (MC state), and the rise corresponds to $D_R q^2$ (SP state) in eqn (1).

To analyze the signal, the diffusion signal is measured at various q^2 values at 3 mM SDS and shown in Fig. 3A. If the light-induced D change occurs on the observation time scale, this process should be considered for the analysis. However, the q^2t plot of the diffusion signal is independent of q^2 (Fig. 3B and SI-2†), indicating that the structural change associated with the photoreaction is completed before the observation time; that is, D is time-independent.

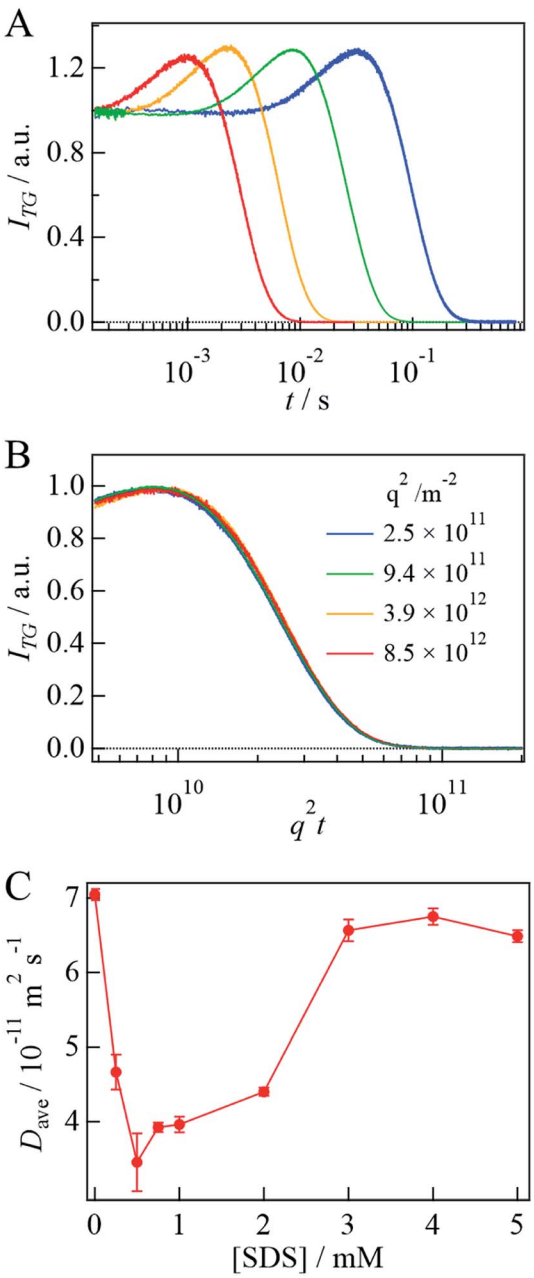

Fig. 3 (A) The q^2 dependence of the diffusion signal of αSynCD at [SDS] = 3 mM and at $q^2 = 8.5 \times 10^{12}$ m^{-2}, 3.9×10^{12} m^{-2}, 9.4×10^{11} m^{-2}, and 2.5×10^{11} m^{-2}, from left to right. (B) q^2t plot of the diffusion profiles of (A). (C) Plot of D_{ave} of αSynCD against [SDS].

Based on these results, the rise-decay profiles should be fitted by eqn (4), which takes into account the diffusion of the reactant and the product;

$$I_{TG} = \alpha\{\delta n_P \exp(-D_P q^2 t) - \delta n_R \exp(-D_R q^2 t) + \delta n_f \exp(-D_f q^2 t)\}^2 \quad (4)$$

where D_f is D of free DSP (3.8×10^{-10} m^2 s^{-1}). We tried to fit the signal using eqn (4). However, since D_P and D_R are not significantly different, D_P and D_R cannot be determined accurately without ambiguity. Even in this case, we found that the averaged values of D_R and D_P ($D_{ave} = (D_R + D_P)/2$) can be determined more accurately by fitting so that we use this averaged value for further discussion. Moreover, we analyzed the concentration-dependent signals by global fitting with a constant $\delta n_P/\delta n_R$ for all data to reduce ambiguity. The TG signals were well reproduced in this manner (Fig. 2C). The concentration dependence of D_{ave} is shown in Fig. 3C. D_{ave} drastically decreased in the [SDS] region of 1–2 mM, and increased from 2 mM to 3 mM. It is interesting to note that the D change region agrees with the CD intensity change region (Fig. 1C). Hence, we consider that D_{ave} decreases by the extended helix formation and increases by the conformational change to the bent-horseshoe helix.

Dynamics of the complex formation by SF-TG

Before the evaluation of kinetic parameters by SF-TG, we determined the dead time of SF-TG under the present experimental conditions. When the delay time after solution mixing is shorter than 100 ms, the decay of the diffusion signal is faster than that in the static condition (Fig. SI-3†). This acceleration is due to the solution turbulence after mixing. At delay times longer than 100 ms, the diffusion signal is almost identical each other. Hence, the dead time is estimated to be 100 ms.

Upon mixing equal volume of the two solutions of 40 μM αSynCD and 6 mM SDS, the final concentration of SDS is rapidly changed to 3 mM, which is sufficiently above the cmc (1.3 mM). Compared to the decay signal of the unfolded state (black line in Fig. 4A), a profile significantly changed at a delay time of 150 ms, at which a rise-decay profile was observed, and then the rise-decay curve gradually changes around 150–5000 ms (Fig. 4A). Since the diffusion time (~10 ms) is sufficiently short compared with the delay time, the signals can be analyzed only by the diffusion process without considering the reaction. The diffusion signals are fitted by eqn (4), and the D_{ave} are plotted against the delay time (Fig. 4B). The observed time dependence of D_{ave} is fitted by a single exponential function. Referring to the intermediate state that appears just after the solution mixing within the dead time of the SF system as an I-state, the D change from the I-state to the final state at the longest delay time is determined to be $(5.5 \pm 0.1) \times 10^{-11}$ m^2 s^{-1} to $(6.9 \pm 0.1) \times 10^{-11}$ m^2 s^{-1} with a rate constant of 0.8(±0.3) s^{-1}. The D of the I-state was smaller than that of the unfolded state ($(7.0 \pm 0.1) \times 10^{-11}$ m^2 s^{-1}), and it increased to the final state of the complex.

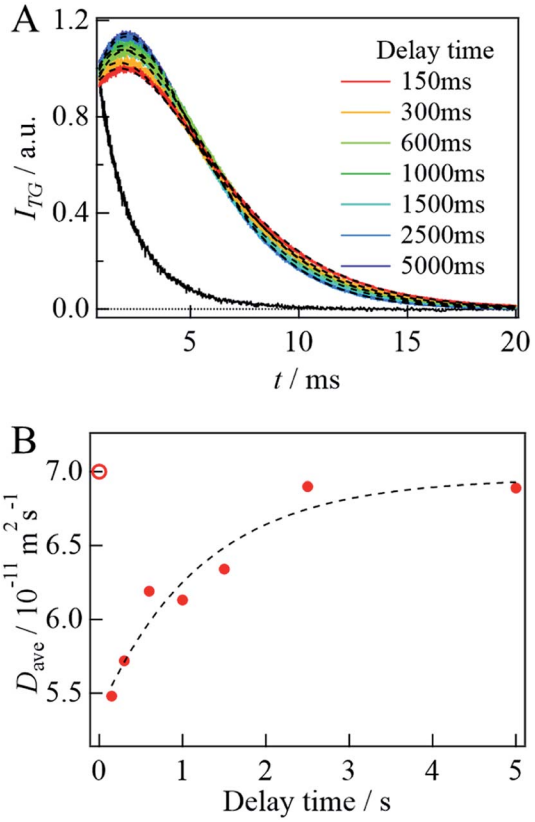

Fig. 4 (A) The delay time dependence of the diffusion signal after mixing αSynCD with SDS solutions at $q^2 = 3.8 \times 10^{12}$ m^{-2}. A black solid line shows the signal obtained by mixing αSynCD with PBS buffer in the absence of SDS at delay time of 5000 ms. The best fitted curves by eqn (4) are shown by the broken lines. (B) Plot of D_{ave} against the delay time (filled circles). The broken line shows a fitted curve by a single exponential function. The calculated D of the unfolded state is shown by an open circle.

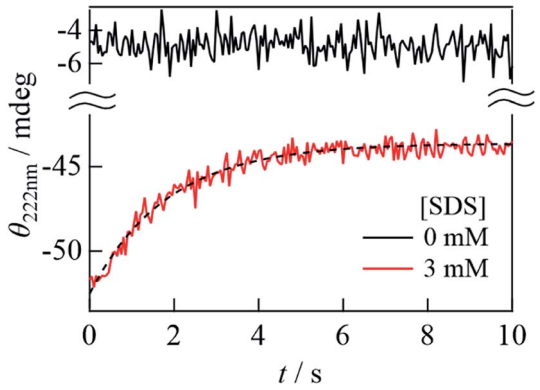

Fig. 5 The time dependence of the CD intensity of αSynC at 222 nm after solution mixing by the SF system (red line). The broken line shows a fitted curve by a single exponential function. The solid black line shows the trace obtained by mixing equal volume of αSynC and PBS buffer in the absence of SDS under the same condition as the SDS mixing.

It should be noted that the initial process completes within the dead time (100 ms).

Detection of secondary structural changes by SF-CD

The secondary structural change dynamics is detected by the SF-CD measurement. When 40 μM αSynC and 6 mM SDS solutions were mixed at a 1 : 1 volume ratio, αSynC exhibited a significant increase in CD signal at 222 nm within a response time of approximately 50 ms (a red line in Fig. 5) compared to the unfolded state (a black line in Fig. 5). Hence, helix formation was completed within the dead time of the measurement. After this initial state, the CD intensity decreased, which suggested that the α-helix content decreased in this time domain. Since CD signal is not observed in the absence of αSynC, the change in CD intensity after mixing of αSynC and SDS is due to the structural change of αSynC. The time profile is fitted by a single exponential function with a rate constant of 0.55(±0.07) s^{-1}. It is interesting to note that this rate is similar to that of the change in D_{ave} obtained by the SF-TG measurement. This result suggests that the helical structure changes at the same time that the complex conformation changes in the transition from the I-state to the final state. The decrease in the helical content is about 20%, which is similar to the CD change from 2 mM to 3 mM SDS (Fig. 1C). Therefore, we consider that the observed change in the CD intensity corresponds to the transition of the N-terminal helical structure from the extended to the horseshoe helix.

Detection of intramolecular structural changes by SF-FRET

Previously, the decrease in the CD intensity at high [SDS] was explained in terms of the bent horseshoe helix formation in the N-terminal region.[19] This suggestion was confirmed by a FRET measurement between two dye molecules located at both ends of the N-terminal helical region (3–92 residues).[19,39] Here, we measured FRET of double-labeled protein at positions 7 and 84 with F488 (donor, $\lambda_{em} = 517$ nm) and F594 (acceptor, $\lambda_{em} = 617$ nm) (Fig. 6A) to examine the time-dependent conformational change detected by TRD and CD methods. If helix bending occurs in the observation time range, the distance between both ends of the helical region becomes short, so that the FRET efficiency increases.

First, the fluorescence spectrum of αSyn labeled only by the acceptor (αSyn-A) is compared with αSyn labeled by the acceptor and donor (αSyn-AD) upon photoexcitation at 449 nm under the same conditions (Fig. 6B). The fluorescence from αSyn-A is very weak, because the absorbance of the acceptor at 449 nm is small. On the contrary, the fluorescence of the acceptor from αSyn-AD is strong. This observation indicates that the excited state energy of the donor is transferred to the acceptor by the FRET process in the buffer without SDS. This result is consistent with those of the previous studies, since the distance between residues of 7 and 84 in the unfolded state is calculated to be ~5 nm and this distance is close enough for FRET (<10 nm).[19,39,40] A similar behavior was also reported in other disordered proteins by single molecule FRET experiments.[41,42]

Next, SDS is added to the solution. For αSyn-A sample, the fluorescence intensity of the acceptor does not change by

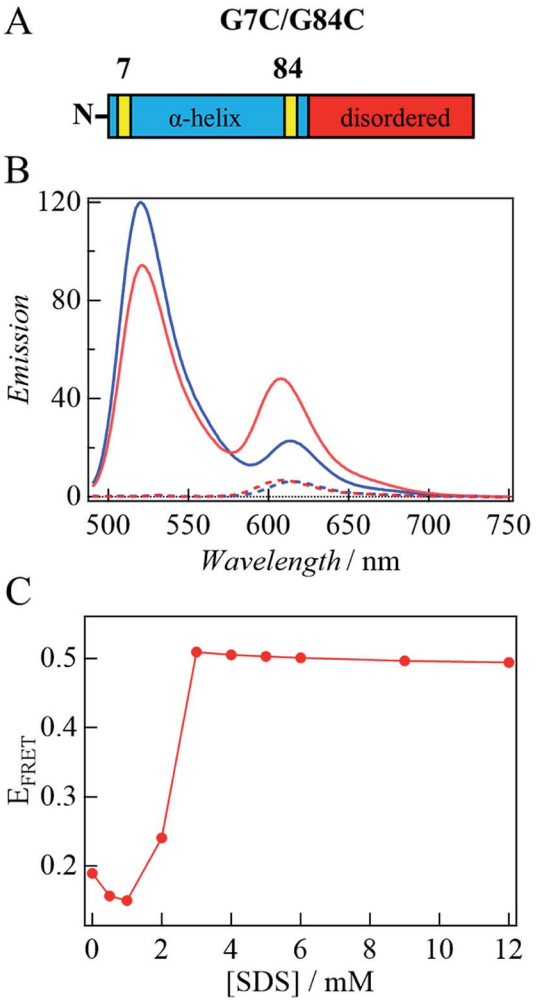

Fig. 6 (A) The domain structure of G7C/G84C. Replaced cysteine residues are shown by the yellow parts. (B) Fluorescence spectrum of αSynAD without SDS (blue) and that at 3 mM SDS upon photoexcitation at 449 nm (red). Broken lines show the spectrum of αSynA upon photoexcitation at 449 nm. (C) Plot of E_{FRET} against [SDS] estimated from the peak intensity.

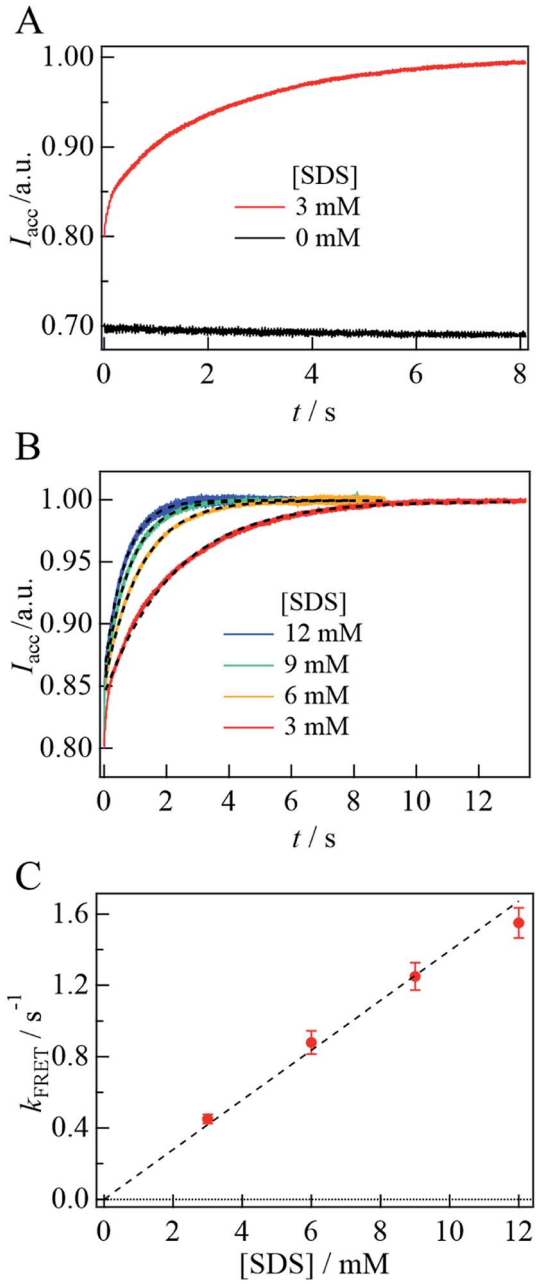

Fig. 7 (A) The kinetic trace of the acceptor fluorescence (I_{acc}) of αSynAD upon photoexcitation at 449 nm after the SDS solution mixing (red). The acceptor fluorescence intensity after the mixing with the PBS buffer without SDS measured under the same condition is shown by the black line. (B) The time dependence of the acceptor fluorescence intensity after the SDS mixing at various [SDS] are fitted by a single exponential function (broken lines). The time traces were normalized by the intensity at the plateau regions. (C) The rate constant of the emission change of the acceptor (k_{FRET}) is plotted against [SDS]. The plot was fitted by a linear function (broken line).

adding SDS. Contrastingly, for the αSyn-AD sample, the donor fluorescence intensity decreases and acceptor fluorescence increases with SDS addition (*e.g.*, 3 mM SDS in Fig. 6B). This suggests that the distance between both ends of the helix decreases. The ratio of the fluorescence peak intensity of the acceptor to that of the donor (E_{FRET}) is plotted against [SDS] (Fig. 6C). It shows that E_{FRET} once decreases at 1 mM SDS and then increases around 2–3 mM, and remains almost constant in the higher concentration region. This trend agrees with previous reports showing the formation of a bent horseshoe helix at high [SDS].[19,39]

Fig. 7A depicts the time dependence of the acceptor fluorescence intensity after solution mixing. Within the dead time of this system (~1 ms), the acceptor fluorescence intensity increases rapidly, and then gradually increase over a time range of several seconds. The gradual change is well reproduced by a single exponential function and the rate constant is determined to be 0.45(±0.03) s^{-1}. With increasing [SDS], the rate of change is found to be faster (Fig. 7B). The fluorescence time trace is reproduced by a single exponential function, and the determined rate constant (k_{FRET}) is plotted against [SDS], as shown in Fig. 7C. We determine the second-order rate constant

from the slope of the plot to be 130 M^{-1} s^{-1}. In the SDS solution at a concentration higher than the cmc, the SDS monomer concentration is considered to be constant and the micelle concentration increases.[43] Since the cmc is 1.3 mM, the SDS dependence of the kinetic trace suggests that helix bending occurs with micelle binding. Assuming that the aggregation number of the micelle is 70,[16] the second-order rate constant on the micelle concentration is 9×10^3 M^{-1} s^{-1}.

Discussion

Before discussing the time-resolved measurements, let us summarize the conformational changes of αSyn interacting with SDS, investigated by TG, CD, and FRET measurements under static conditions. In the transition from the absence of SDS to the [SDS] range of 1–2 mM, the CD intensity increases significantly (Fig. 1C), D decreases by approximately half (Fig. 3C), and E_{FRET} slightly decreases at 1 mM, followed by a slight increase at 2 mM (Fig. 6C). According to previous studies, these changes can be explained as follows. While the αSyn structure is unfolded in the buffer without SDS, the increase in the CD intensity indicates α-helix formation upon interaction with SDS. The decrease in D represents the increase in the size of αSyn due to the formation of the αSyn–SDS complex. Previously, it has been reported that D of an unfolded protein is about 1.5–2 times smaller compared with that of the folded protein[44,45] because of the intermolecular hydrogen bonding between the protein and water.[44] Hence, the decrease in D accompanying the formation of α-helix should be explained in terms of the increase in the size by the SDS complex formation to compensate for the decrease in the diffusion friction due to α-helix formation. An NMR structural analysis of the complex showed that while the N-terminal region is bound to the SDS micelle and forms a helical structure, the region after Gly^{93} is unbound to the micelle and unstructured, and the region of Asp^{98}–Ala^{140} has highly mobile fluctuations.[21] Therefore, the effect of the formation of the helical structure might be relatively smaller than in the case of complete folding of a protein. The slight decrease in E_{FRET} at 1 mM indicates that the distance between residues 7 and 84 is longer than that in the unfolded state. We consider that this distance in the unfolded state is rather short due to a compact structure for FRET, whereas the distance is expected to be long in an extended α-helix form. Therefore, the origin of the slight decrease in E_{FRET} is attributed to the extended α-helix formation. Even in this state, E_{FRET} is not zero. This non-zero E_{FRET} in the extended form has been observed previously[19] and this observation implies that the distance between 7 and 84 is not long enough for negligible FRET. However, we cannot exclude another possibility, *i.e.*, a conformational heterogeneity at 1 mM SDS. It may be reasonable to consider that αSyn is in equilibrium between the extended and the micelle-bound-horseshoe helix near the cmc. In the horseshoe helix, the distance should be shorter than that in the extended helix, and a small amount of the horseshoe component contributes to the non-zero FRET at 1 mM SDS. With increasing [SDS], the E_{FRET} increases, suggesting that a bending of the α-helix is dominant.

When [SDS] is increased to more than 3 mM, the CD intensity slightly decreases, D increases to almost that in the buffer solution, and E_{FRET} also increases. The slight decrease in the CD intensity can be explained by the bent horseshoe α-helix structure. This interpretation is consistent with the increase in E_{FRET}. The increase in D could be explained by two effects: D decreases due to complex formation with SDS micelles, and increases when the protein conformation on the SDS surface becomes compact. A previous small-angle X-ray scattering (SAXS) study has reported that the maximum diameter of αSyn having an elongated helix is 1.5–2 times larger than that of the complex with the bent helix on the micelle.[16] In this study, D_{ave} obtained from TG at 3 mM or higher [SDS] is 1.5 times larger than that in the 1–2 mM concentration range. Although there is no direct relationship between the maximum diameter estimated from SAXS measurements and the hydrodynamic radius from the diffusion measurement, it is interesting to find that these factors agree well. Furthermore, a previous study reported deformation of the globular micelle with protein binding.[21] This deformation of the micelle shape may also contribute to the increase in D.

The time-resolved measurements, in combination with the SF system, revealed the kinetics of the conformational change and binding of αSyn on the SDS micelles. According to the SF-CD measurement, the CD intensity dramatically increased within the response time of 50 ms, followed by a slight decrease toward the final state. These changes seem to be similar to the changes observed in the [SDS] dependence experiment from the diluted to concentrated SDS conditions (Fig. 1C). Although this coincidence could be accidental, it may be reasonable to explain the observed time dependence by a process from the I-state possessing an extended α-helix in the N-terminal region to a final bent α-helix form (product).

The SF-FRET experiments showed that the FRET efficiency of the fluorescent molecules labeled on both ends of the N-terminal helix (position 7 and 84) increases within 1 ms of the addition of the SDS solution and further increased gradually. This result indicates that a rather compact α-helix formation is completed within 1 ms upon interaction with the SDS molecules and that the average distance between both ends of the N-terminal helix becomes shorter. Since E_{FRET} at 1 ms is larger than that at 0 mM (Fig. 7A), the I-state could be slightly bent from the extended α-helix. Another possible origin is the heterogeneous contributions of the extended α-helix and the compact helix form, which is described above for the 1 mM SDS concentration. If both conformations are formed in the I-state, it may be reasonable to observe the slight increase in the FRET efficiency. After this process, the helix bent further by forming a complex with the SDS micelle on a time scale of several seconds, which is confirmed by the SF-CD signals. Interestingly, the rate of change is proportional to the micelle concentration, *i.e.*, this step is the second-order reaction, suggesting that αSyn is transferred to the micelle to form the final product. Hence, αSyn does not interact with the micelle before this final state, but we speculate that αSyn interacts with the SDS monomers to form the extended α-helix conformation in the I-state.

The SF-TG experiments provide information on the change in the hydrodynamic radius. The observed time dependence indicates that D of the intermediate decreased from the unfolded state significantly, followed by an increase toward the micelle-bound state. As described above, D of the folded protein is larger than that of the unfolded protein in many cases. The decrease in D in the I-state may be an indication of the intermolecular interaction with many SDS monomers to form large aggregates. The increase in D after the formation of the final product, the αSyn–micelle complex, could be due to a compact (bend α-helix) form on the micelle after the transport from the SDS aggregates to the micelle.

There may be several explanations for the slow αSyn–micelle complex formation. It has been shown that at high [SDS], the N-terminal helix of αSyn is slightly embedded inside the micelle.[21] The positively charged residues of the amphipathic N-terminal helix can interact with the negatively charged headgroups of SDS. Contrastingly, the inner helix, which is largely hydrophobic, interacts with the hydrophobic moiety of the SDS tails. If αSyn is surrounded by many SDS monomers in the I-state, as we suggested, these monomers must be released from αSyn before forming the complex with the micelle. This process could be slow. It has also been reported that the interaction of αSyn with the micelle leads to shape deformation of the micelle to a prolate ellipsoidal structure.[21] Hence, the complex formation between αSyn and micelles results in not only structural changes in the conformation of αSyn, but also deformation of the micelle. These changes may also cause a slow transition from the intermediate to the final state in the binding reaction. The proposed reaction scheme based on the above considerations is shown in Fig. 8.

Previous studies using molecular dynamics (MD) simulations suggested an assembly of SDS monomers in the presence of αSyn occurs within 100 ns.[46] However, a stable helix formation was not observed within hundreds of nanoseconds simulation. Our results indicate that the formation of the extended helix is completed in the microsecond time scale. In the binding reaction, this intermediate interacts with the micelle, and the helix bending induced by binding to the micelle slowly proceeds in a time range of several seconds. In the MD simulation study, the αSyn–micelle complex formation was simulated, and the binding movement was observed within approximately 100 ns.[46] However, in the present experimental study, the association of αSyn with the micelle occurred within a few seconds. This difference might be due to a simplified MD simulation, which was carried out by assuming no SDS monomers present in the initial state.

So far, SDS has been used to mimic interaction between αSyn and membrane in many studies. However, using lipid vesicles is also appropriate to understand the biological role of αSyn in cells. In fact, it has been reported that αSyn with lipid vesicles exhibits both the extended and the horseshoe helices and the extended form may be a major component.[11] Our techniques presented here, in particular SF-TG method, can be used under such conditions.

Summary

The conformational change dynamics of αSyn induced by interaction with SDS micelles are studied in the time domain. The TRD measurement based on the TG detection as well as SF-CD, and SF-FRET experiments reveal the time course of the conformational change of αSyn upon interaction with SDS. Initially, the elongated helix was formed within 1 ms (the I-state) in the process of the interaction with many SDS monomers. The intermediate bound to the micelle with the second-order rate constant for [SDS]. We propose that the α-helix formation is completed by binding to the SDS monomers, followed by association with the micelle to form the bend structure.

In this study, we also demonstrate that the μ-SF system we used for the detection by TG and FRET is very useful for the time-resolved studies of a sample that can be prepared only in minimal amounts, such as proteins. In particular, the time-resolved diffusion technique is a promising method for studies on protein reactions because D is sensitive to conformation changes, intermolecular interactions, and changes in size by forming protein complexes. It has been very difficult to detect the dynamics of these properties using other time-resolved measurements, such as CD and fluorescence measurements. For example, although the CD intensity reflects the secondary structure, the association/dissociation processes or intermolecular interaction cannot be detected by this method. The FRET experiment is powerful for detecting the distance change between the donor and acceptor, but it cannot detect again the other processes. In our previous paper, we demonstrated that the SF-TG technique is applicable to a pH jump experiment for a photoreactive protein. The present study

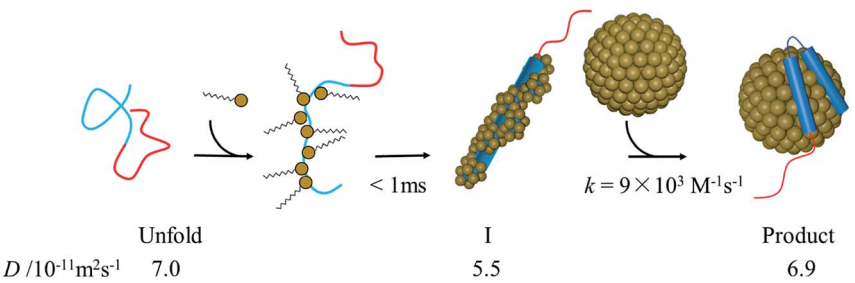

Fig. 8 Illustration of proposed reaction scheme of αSyn–SDS interaction.

is the first application of a reaction to a non-photoreactive protein. This novel method is a promising tool for studying protein interactions such as enzymatic reactions.

Conflicts of interest

There are no conflicts to declare.

Acknowledgements

This work was supported by a Grant-in-aid for Scientific Research on Innovative Areas (research in a proposed research area) (No. JP20107003, and JP25102004 to M. T.), a Grant-in-aid for Scientific Research from MEXT/JSPS (25288005, 17H03008 to M. T., 17H05001 and 20H04708 to Y. N.), and Research Foundation for Opto-Science and Technology (to M. T.)

References

1 P. H. Weinreb, W. Zhen, A. W. Poon, K. A. Conway and P. T. Lansbury Jr, NACP, A Protein Implicated in Alzheimer's Disease and Learning, Is Natively Unfolded, *Biochemistry*, 1996, **35**, 13709–13715.

2 L. Maroteaux, J. T. Campanelli and R. H. Scheller, Synuclein: A Neuron-Specific Protein Localized to the Nucleus and Presynaptic Nerve Terminal, *J. Neurosci.*, 1988, **8**, 2804–2815.

3 L. Breydo, J. W. Wu and V. N. Uversky, α-Synuclein misfolding and Parkinson's disease, *Biochim. Biophys. Acta, Mol. Basis Dis.*, 2012, **1822**, 261–285.

4 B. Fauvet, M. K. Mbefo, M.-B. Fares, C. Desobry, S. Michael, M. T. Ardah, E. Tsika, P. Coune, M. Prudent, N. Lion, D. Eliezer, D. J. Moore, B. Schneider, P. Aebischer, O. M. El-Agnaf, E. Masliah and H. A. Lashuel, α-Synuclein in Central Nervous System and from Erythrocytes, Mammalian Cells, and *Escherichia coli* Exists Predominantly as Disordered Monomer, *J. Biol. Chem.*, 2012, **287**, 15345–15364.

5 M. H. Polymeropoulos, C. Lavedan, E. Leroy, S. E. Ide, A. Dehejia, A. Dutra, B. Pike, H. Root, J. Rubenstein, R. Boyer, E. S. Stenroos, S. Chandrasekharappa, A. Athanassiadou, T. Papapetropoulos, W. G. Johnson, A. M. Lazzarini, R. C. Duvoisin, G. Di Iorio, L. I. Golbe and R. L. Nussbaum, Mutation in the α-synuclein gene identified in families with Parkinson's disease, *Science*, 1997, **276**, 2045–2047.

6 R. Kruger, W. Kuhn, T. Muller, D. Woitalla, M. Graeber, S. Kosel, H. Przuntek, J. T. Epplen, L. Schols and O. Riess, Ala30Pro mutation in the gene encoding α-synuclein in Parkinson's disease, *Nat. Genet.*, 1998, **18**, 106–108.

7 H. A. Lashuel, C. R. Overk, A. Oueslati and E. Masliah, The many faces of α-synuclein: from structure and toxicity to therapeutic target, *Nat. Rev. Neurosci.*, 2013, **14**, 38–48.

8 N. Bengoa-Vergniory, R. F. Roberts, R. Wade-Martins and J. Alegre-Abarrategui, Alpha-synuclein oligomers: a new hope, *Acta Neuropathol.*, 2017, **134**, 819–838.

9 C. M. Pfefferkorn, Z. Jiang and J. C. Lee, Biophysics of α-synuclein membrane interactions, *Biochim. Biophys. Acta, Biomembr.*, 2012, **1818**, 162–171.

10 A. Iyer and M. M. A. E. Claessens, Disruptive membrane interactions of alpha-synuclein aggregates, *Biochim. Biophys. Acta, Proteins Proteomics*, 2019, **1867**, 468–482.

11 S. Bekshe Lokappa and T. S. Ulmer, α-Synuclein populates both elongated and broken helix states on small unilamellar vesicles, *J. Biol. Chem.*, 2011, **286**, 21450–21457.

12 C. C. Jao, A. Der-Sarkissian, J. Chen and R. Langen, Structure of membrane-bound-synuclein studied by site-directed spin labeling, *Proc. Natl. Acad. Sci. U. S. A.*, 2004, **101**, 8331–8336.

13 M. Rovere, A. E. Powers, H. Jiang, J. C. Pitino, L. Fonseca-Ornelas, D. S. Patel, A. Achille, R. Langen, J. Varkey and T. Bartels, E46K-like α-synuclein mutants increase lipid interactions and disrupt membrane selectivity, *J. Biol. Chem.*, 2019, **294**, 9799–9812.

14 S. Chandra, X. Chen, J. Rizo, R. Jahn and T. C. Südhof, A broken α-helix in folded α-synuclein, *J. Biol. Chem.*, 2003, **278**, 15313–15318.

15 A. C. M. Ferreon and A. A. Deniz, α-Synuclein multistate folding thermodynamics: implications for protein misfolding and aggregation, *Biochemistry*, 2007, **46**, 4499–4509.

16 L. Giehm, C. L. P. Oliveira, G. Christiansen, J. S. Pedersen and D. E. Otzen, SDS-Induced Fibrillation of α-Synuclein: An Alternative Fibrillation Pathway, *J. Mol. Biol.*, 2010, **401**, 115–133.

17 M. F. Ahmad, T. Ramakrishna, B. Raman and C. M. Rao, Fibrillogenic and Non-Fibrillogenic Ensembles of SDS-Bound Human α-Synuclein, *J. Mol. Biol.*, 2006, **364**, 1061–1072.

18 D. Ruzafa, Y. S. Hernandez-Gomez, G. Bisello, K. Broersen, B. Morel and F. Conejero-Lara, The influence of N-terminal acetylation on micelle-induced conformational changes and aggregation of α-Synuclein, *PLoS One*, 2017, **12**, e0178576.

19 A. C. M. Ferreon, Y. Gambin, E. A. Lemke and A. A. Deniz, Interplay of α-synuclein binding and conformational switching probed by single-molecule fluorescence, *Proc. Natl. Acad. Sci. U. S. A.*, 2009, **106**, 5645–5650.

20 E. R. Georgieva, T. F. Ramlall, P. P. Borbat, J. H. Freed and D. Eliezer, The lipid-binding domain of wild type and mutant α-synuclein: Compactness and interconversion between the broken and extended helix forms, *J. Biol. Chem.*, 2010, **285**, 28261–28274.

21 T. S. Ulmer, A. Bax, N. B. Cole and R. L. Nussbaum, Structure and dynamics of micelle-bound human α-synuclein, *J. Biol. Chem.*, 2005, **280**, 9595–9603.

22 M. Terazima, Time-dependent intermolecular interaction during protein reactions, *Phys. Chem. Chem. Phys.*, 2011, **13**, 16928–16940.

23 T. Brand, E. J. Cabrita and S. Berger, Intermolecular interaction as investigated by NOE and diffusion studies, *Prog. Nucl. Magn. Reson. Spectrosc.*, 2005, **46**, 159–196.

24 M. Terazima, Studies of photo-induced protein reactions by spectrally silent reaction dynamics detection methods:

applications to the photoreaction of the LOV2 domain of phototropin from *Arabidopsis thaliana*, *Biochim. Biophys. Acta, Proteins Proteomics*, 2011, **1814**, 1093–1105.

25 K. Tanaka, Y. Nakasone, K. Okajima, M. Ikeuchi, S. Tokutomi and M. Terazima, Light-induced conformational change and transient dissociation reaction of the BLUF photoreceptor *Synechocystis* PixD (Slr1694), *J. Mol. Biol.*, 2011, **409**, 773–785.

26 M. Kondoh and M. Terazima, Conformational and Intermolecular Interaction Dynamics of Photolyase/Cryptochrome Proteins Monitored by the Time-Resolved Diffusion Technique, *Photochem. Photobiol.*, 2017, **93**, 15–25.

27 A. Takakado, Y. Nakasone and M. Terazima, Sequential DNA Binding and Dimerization Processes of the Photosensory Protein EL222, *Biochemistry*, 2018, **57**, 1603–1610.

28 Y. Nakasone, S. Takaramoto and M. Terazima, Time-Resolved Diffusion Detection with Microstopped Flow System, *Anal. Chem.*, 2019, **91**, 11987–11993.

29 N. Baden and M. Terazima, A novel method for measurement of diffusion coefficients of proteins and DNA in solution, *Chem. Phys. Lett.*, 2004, **393**, 539–545.

30 R. Klajn, Spiropyran-based dynamic materials, *Chem. Soc. Rev.*, 2014, **43**, 148–184.

31 S. Takaramoto, Y. Nakasone, K. Sadakane, S. Maruta and M. Terazima, Spiropyran labeling for sensitive probing of protein diffusion by the transient grating method, *Chem. Phys. Lett.*, 2020, **739**, 136919.

32 C. Huang, G. Ren, H. Zhou and C. C. Wang, A new method for purification of recombinant human α-synuclein in *Escherichia coli*, *Protein Expression Purif.*, 2005, **42**, 173–177.

33 M. Terazima and N. Hirota, Measurement of the quantum yield of triplet formation and short triplet lifetimes by the transient grating technique, *J. Chem. Phys.*, 1991, **95**, 6490–6495.

34 M. Terazima, Diffusion coefficients as a monitor of reaction kinetics of biological molecules, *Phys. Chem. Chem. Phys.*, 2006, **8**, 545–557.

35 R. M. Weinheimer, D. Fennell Evans and E. L. Cussler, Diffusion in Surfactant Solutions, *J. Colloid Interface Sci.*, 1981, **80**, 357–368.

36 G. Manzo, M. Carboni, A. C. Rinaldi, M. Casu and M. A. Scorciapino, Characterization of sodium dodecylsulphate and dodecylphosphocholine mixed micelles through NMR and dynamic light scattering, *Magn. Reson. Chem.*, 2013, **51**, 176–183.

37 Y. Wang, L. A. Benton, V. Singh and G. J. Pielak, Disordered protein diffusion under crowded conditions, *J. Phys. Chem. Lett.*, 2012, **3**, 2703–2706.

38 J. Bai, Z. Zhang, M. Liu and C. Li, α-Synuclein–lanthanide metal ions interaction: binding sites, conformation and fibrillation, *BMC Biophys.*, 2016, **9**, 1.

39 G. Veldhuis, I. Segers-Nolten, E. Ferlemann and V. Subramaniam, Single-molecule FRET reveals structural heterogeneity of SDS-bound α-synuclein, *ChemBioChem*, 2009, **10**, 436–439.

40 S. S. Vogel, B. W. Van der Meer and P. S. Blank, Estimating the distance separating fluorescent protein FRET pairs, *Methods*, 2014, **66**, 131–138.

41 S. Mukhopadhyay, R. Krishnan, E. A. Lemke, S. Lindquist and A. A. Deniz, A natively unfolded yeast prion monomer adopts an ensemble of collapsed and rapidly fluctuating structures, *Proc. Natl. Acad. Sci. U. S. A.*, 2007, **104**, 2649–2654.

42 G. N. W. Gomes, M. Krzeminski, A. Namini, E. W. Martin, T. Mittag, T. Head-Gordon, J. D. Forman-Kay and C. C. Gradinaru, Conformational Ensembles of an Intrinsically Disordered Protein Consistent with NMR, SAXS, and Single-Molecule FRET, *J. Am. Chem. Soc.*, 2020, **142**, 15697–15710.

43 E. Kudryashov, T. Kapustina, S. Morrissey, V. Buckin and K. Dawson, The Compressibility of Alkyltrimethylammonium Bromide Micelles, *J. Colloid Interface Sci.*, 1998, **203**, 59–68.

44 S. Nishida, T. Nada and M. Terazima, Kinetics of intermolecular interaction during protein folding of reduced cytochrome c, *Biophys. J.*, 2004, **87**, 2663–2675.

45 K. Chattopadhyay, S. Saffarian, E. L. Elson and C. Frieden, Measuring unfolding of proteins in the presence of denaturant using fluorescence correlation spectroscopy, *Biophys. J.*, 2005, **88**, 1413–1422.

46 J. Tian, A. Sethi, D. Anunciado, D. M. Vu and S. Gnanakaran, Characterization of a disordered protein during micellation: Interactions of α-synuclein with sodium dodecyl sulfate, *J. Phys. Chem. B*, 2012, **116**, 4417–4424.